


Reconstructed conventional bulk-boundary correspondence in the non-Hermitian s -wave nodal-ring superconductor

Chunhui Zhang¹, Li Sheng,^{*} and Dingyu Xing

*National Laboratory of Solid State Microstructures, Department of Physics,
and Collaborative Innovation Center of Advanced Microstructures, Nanjing University, Nanjing 210093, China*

 (Received 9 June 2021; revised 29 August 2021; accepted 7 September 2021; published 16 September 2021)

Recently, the interplay between the non-Hermitian skin effect (NHSE) and topological phases has attracted a lot of attention. When the NHSE occurs in a topological system, the conventional bulk-boundary correspondence (BBC) based on the Bloch band theory is destroyed. In this work, we investigate a non-Hermitian nodal-ring semimetal with the s -wave superconducting (SC) term. We find that the SC term introduces the intrinsic coupling between the different general Brillouin zones (GBZs) of the particle and hole subbands in our model, which drives the total GBZ to the BZ. Furthermore, when the SC term is finite, we show a possibility that the GBZ is the same as the BZ. We also find that the Bloch winding number of the quasi-one-dimensional model can predict the number of Majorana zero states faithfully in this case, which implies that the conventional BBC is reconstructed in our model. The localization strengths of the Majorana zero states are also calculated to show the reconstruction of conventional BBC. The finite-size effect, related experimental regimes in the electric circuit, and the fragility of this reconstructed conventional BBC are also discussed in this work.

DOI: [10.1103/PhysRevB.104.104508](https://doi.org/10.1103/PhysRevB.104.104508)

I. INTRODUCTION

In the past few decades, Hermitian topological materials [1–3], including topological insulators [1,2,4–11], topological superconductors [1,2,12–24] and topological semimetals [25–39], have been intensively studied. For these topological systems, one of the most important features is that they possess conventional bulk-boundary correspondence (BBC), i.e., the topological boundary modes can be characterized by the bulk topological invariants based on the Bloch Hamiltonians.

Besides, recently the non-Hermiticity has been introduced in many physical systems, like open quantum systems [40–46], cold-atom systems [47–53], and condensed matter systems [54–59]. For many non-Hermitian systems, the non-Hermitian skin effect (NHSE) is important because it makes the energy spectrum under open boundary conditions (OBC) different from one under periodic boundary conditions (PBC) [60–66]. To understand this phenomenon, the Brillouin zone (BZ) is generalized to the generalized Brillouin zone (GBZ) [65–69]. As long as the NHSE exists in a non-Hermitian system, the GBZ will be different from BZ, and the energy spectrums under PBC and OBC will be distinct from each other [68].

For a non-Hermitian system with nontrivial topology, the NHSE leads to the destruction of the conventional BBC, which means that the Bloch topological invariant cannot predict the number of zero edge modes precisely. And the correct BBC is based on the GBZ and the non-Bloch band theory [60–63,67–76]. This conclusion motivates us that if the NHSE is removed, the Bloch topological invariant gives the correct phase boundary and the conventional BBC is reconstructed,

which can be realized by making the GBZ coincide with the BZ. To this aim, we can couple different GBZs in a model, which means that the two different localized eigenstates due to the NHSE are also coupled. This method has been applied to construct models with the critical NHSE (CNHSE) very recently [77,78]. In this paper, we consider a non-Hermitian nodal-ring semimetal with the s -wave superconducting (SC) pairing term. Figure 1 is the schematic for the effectively removed NHSE, and the reconstructed conventional BBC: Distinct from the previous CNHSE models [77,78], the coupling between different NHSE localizations is *intrinsic* in our model. i.e., The SC pairing term introduces the particle and hole subbands with different NHSE localizations. Meanwhile, since the two subbands are coupled by the SC term, the different NHSE localizations in particle and hole parts are also coupled. By numerically calculating the GBZ, we show a possibility that the coupling effect of different sub-GBZs drives them to the BZ. For the finite SC term, the GBZ will be almost the same as the BZ, which indicates that the two different NHSE localizations in the particle and hole parts are perfectly canceled and the NHSE in our model is effectively removed. In this case, we find that the Bloch winding number can predict the topological phase transition correctly, and the conventional BBC is reconstructed.

This work is organized as follows: In Sec. II we review the NHSE in the non-Hermitian nodal-ring semimetal. Some introductions about the concepts in non-Hermitian topological physics (such as the GBZ, the NHSE, and the non-Bloch topological invariant) are also included in this section. In Sec. III we introduce our non-Hermitian nodal-ring semimetal model with the s -wave pairing term and discuss its symmetry, topological class, and the Bloch topological invariant. In Sec. IV we show that the sub-GBZs corresponding to the particle and hole subbands are coupled by the nonzero SC

^{*} shengli@nju.edu.cn

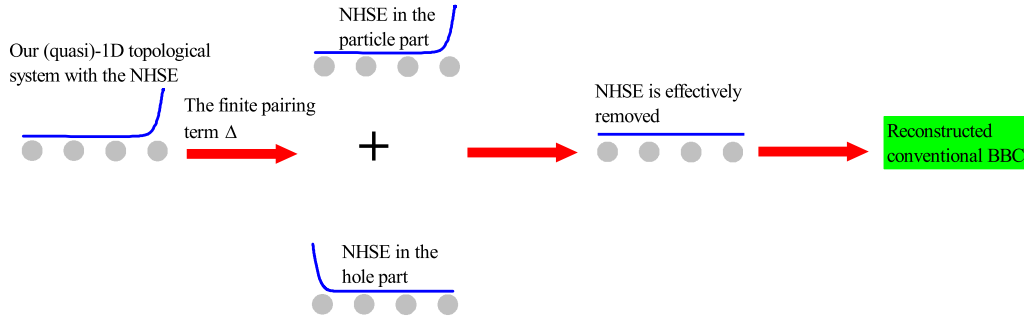


FIG. 1. Schematic for the effectively removed NHSE and the reconstructed conventional BBC. The blue curves and lines denote an eigenstate. Since our quasi-1D model possesses the NHSE, after adding the finite SC pairing term, an eigenstate of the particle part tends to be localized at one edge of the system, and the corresponding eigenstate of the hole part tends to be localized at another edge of the system. i.e., the particle and hole parts have different localized eigenstates due to the NHSE. Meanwhile, the two parts are coupled by the SC pairing term Δ . If such two NHSE localizations cancel each other, the NHSE can be effectively removed in our system. This makes the Bloch topological invariant give the correct phase boundary again, which indicates that the conventional BBC is reconstructed.

pairing term and they are driven to BZ with an increasing SC pairing term. We also find that the GBZ and BZ are the same when the SC pairing term is finite, which indicates that the NHSE is effectively removed. Then in Sec. V, we show that the conventional BBC is reconstructed with the finite SC pairing term by calculating the Bloch and real-space winding numbers, the spectrum under OBC, topological edge modes, and localization strengths of Majorana zero modes. The finite-size effect of our model is discussed in Sec. VI. Next, we give a possible electric circuit realization of our model in Sec. VII. Finally, we discuss some more general cases of our model and make conclusions in Sec. VIII.

II. REVIEW OF THE NON-HERMITIAN NODAL-RING SEMIMETAL

In this section, we review the NHSE and GBZ in the non-Hermitian nodal-ring semimetal [71]. During this process, we will also introduce the important concepts in non-Hermitian physics, including the NHSE, the GBZ, and the non-Bloch winding number.

Let us consider the following model describing the non-Hermitian nodal-ring semimetal:

$$H_0(\mathbf{k}_{\parallel}, k_z) = \left(m + 2B \sum_{i=x,y,z} \cos k_i \right) \sigma_x + (i\gamma + v_z \sin k_z) \sigma_z, \quad (1)$$

where $\mathbf{k}_{\parallel} = (k_x, k_y)$, Pauli matrices $\sigma_{x,y,z}$ act on the spin degree of freedom, and v_z is the Fermi velocity along the z direction; $m \geq 0$ and $B > 0$ are model parameters about the material. Since we focus on the BBC, we regard k_x and k_y as parameters and take the OBC along the z direction, then the non-Hermitian nodal-ring semimetal can be regarded as a quasi-one-dimensional (quasi-1D) system. The corresponding quasi-1D lattice model of Eq. (1) is:

$$H_0 = \sum_{j,s}^L (m_{xy} c_{j,s}^{\dagger} c_{j,-s} + i\gamma s c_{j,s}^{\dagger} c_{j,s}) + \sum_{j,s}^{L-1} \left[B(c_{j,s}^{\dagger} c_{j+1,-s} + h.c.) - \frac{1}{2} i(v_z s c_{j,s}^{\dagger} c_{j+1,s} - H.c.) \right], \quad (2)$$

where $m_{xy} = m + 2B(\cos k_x + \cos k_y)$, j is the lattice index along the z direction, $s = 1(-1)$ denotes the spin up (spin down), and we omit the k_x and k_y indexes in the fermion operators.

Then we assume a trial function of the n_z th site along the z direction $\psi(\mathbf{k}_{\parallel}, n_z) = e^{i(k_x x + k_y y)} (\alpha_1, \alpha_2)^T \beta^{n_z}$ and substitute it to Eq. (2). Then, we can obtain the eigenvalue equation of the bulk part:

$$\begin{bmatrix} E - i\gamma + \frac{iv_z}{2}(\beta - \beta^{-1}) & -m_{xy} - B(\beta + \beta^{-1}) \\ -m_{xy} - B(\beta + \beta^{-1}) & E + i\gamma - \frac{iv_z}{2}(\beta - \beta^{-1}) \end{bmatrix} \begin{bmatrix} \alpha_1 \\ \alpha_2 \end{bmatrix} = [EI - H_0(\mathbf{k}_{\parallel}, \beta)]\alpha = 0, \quad (3)$$

where I is the 2×2 identity matrix and $\alpha = [\alpha_1, \alpha_2]^T$. We note that $H_0(\mathbf{k}_{\parallel}, \beta)$ in the second line of Eq. (3) can be obtained by making the replacement $e^{ik_z} \rightarrow \beta$ in Eq. (1). So the eigenvalue equation of $H_0(\mathbf{k}_{\parallel}, \beta)$ is exactly the second line of Eq. (3). To ensure that Eq. (3) has nontrivial solutions, we have

$$\det[EI - H_0(\mathbf{k}_{\parallel}, \beta)] = 0, \quad (4)$$

where I is the 2×2 identity matrix. Then we have

$$E^2 = \left[m_{xy} + B \left(\beta + \frac{1}{\beta} \right) \right]^2 + \left[\frac{v_z}{2i} \left(\beta - \frac{1}{\beta} \right) + i\gamma \right]^2. \quad (5)$$

In this section, for simplicity we consider $B = v_z/2 = t$, then the equation is

$$2t(m_{xy} + \gamma)\beta^2 + (m_{xy}^2 - \gamma^2 + 4t^2 - E^2)\beta + 2t(m_{xy} - \gamma) = 0, \quad (6)$$

so the two solutions of Eq. (6) β_1 and β_2 satisfy

$$\beta_1 \beta_2 = \frac{m_{xy} - \gamma}{m_{xy} + \gamma}. \quad (7)$$

Note that this quasi-1D model has the sublattice symmetry (SLS) $\sigma_y H_0 \sigma_y^{-1} = -H_0$, according to the results in Refs. [67,69], the boundary conditions $\psi(k_{\parallel}, 0) = \psi(k_{\parallel}, L+1) = 0$ lead to $|\beta_1| = |\beta_2|$ in a 1D non-Hermitian system with the SLS. Combining with Eq. (B4), we obtain that

$$|\beta| = |\beta_1| = |\beta_2| = \sqrt{\left| \frac{m_{xy} - \gamma}{m_{xy} + \gamma} \right|}, \quad (8)$$

and the the solution of β is

$$\beta(k_z) = \sqrt{\left| \frac{m_{xy} - \gamma}{m_{xy} + \gamma} \right|} e^{ik_z}, \quad (9)$$

with $k_z \in [-\pi, \pi]$.

We first focus on the *Hermitian case* $\gamma = 0$. From Eq. (9) we find that $\beta(k_z) = e^{ik_z}$ and $k_z \in [-\pi, \pi]$ exactly correspond to the Bloch wave vector and the traditional BZ for 1D systems (we have regarded the k_x and k_y as parameters).

Next, if m_{xy} and γ are nonzero, then we write Eq. (9) as $\beta(k_z) = e^{i(k_z - i \ln r)}$ with

$$r = \frac{1}{2} \ln \left| \frac{m_{xy} - \gamma}{m_{xy} + \gamma} \right|, \quad (10)$$

with $k_z \in [-\pi, \pi]$. We can see that the Bloch vector k_z is replaced by the “complex non-Bloch wave vector” $k_z - i \ln r$. And the imaginary part of the complex non-Bloch vector leads to the exponential-decay behavior, then *all* of the eigenstates become localized. This localization behavior is dubbed as the NHSE [61]. Besides, the solution β is a complex function about the k and has a trajectory C_β in the complex β plane. In non-Hermitian physics, this solution $\beta(k_z) = e^{i(k_z - i \ln r)}$ or its trajectory C_β is also dubbed as GBZ [61,67,69].

Next we consider the $H_0(\mathbf{k}_\parallel, \beta)$, if $\beta = \beta_0 = e^{ik_z}$, then we can obtain Eq. (1) again. Since the k_z is the Bloch wave vector, Eq. (1), is a Bloch Hamiltonian. However, as we have shown in above, the correct solution β corresponding to the eigenenergies and eigenstates under the OBC usually contains the non-Bloch wave vector $k_z - i \ln r$. In these cases, $H_0(\mathbf{k}_\parallel, \beta)$ is dubbed as the non-Bloch Hamiltonian. Based on the Bloch (non-Bloch) Hamiltonian, we can obtain the Bloch (non-Bloch) winding number W_{k_z} (W_β). However, since the β corresponds to the eigenenergies and eigenstates under the OBC, only the W_β [61,67,71] or real-space winding number (dual to the non-Bloch winding number [75]) can give the correct BBC in this model.

In the final part of this section, we want to give several notes: Since we have set $2B = v_z$, the characteristic equation, Eq. (4), about β only has two solutions and they can be easily and analytically solved. However, in most non-Hermitian models, there are m solutions of β with $|\beta_1| \leq |\beta_2| \leq \dots \leq |\beta_{m-1}| \leq |\beta_m|$. For a non-Hermitian system with the SLS, it has been found that m is an even number and the GBZ is given by $|\beta| = |\beta_{m/2}| = |\beta_{m/2+1}| = e^{i[k - i \ln r_k]}$ or the corresponding trajectory C_β [67,69]. Unlike the result in Eq. (9), the exponential-decay part in the non-Bloch wave vector is also a function of k , and solving the r_k analytically is very difficult. To solve this β , we can straightforwardly obtain the energies E of the lattice Hamiltonian under the OBC. After substituting each E to the characteristic equation like Eq. (4), we can numerically solve the β and obtain the GBZ [61]. Besides, recently the auxiliary GBZ method has been proposed [69], which works well for the lattice strength $L \rightarrow \infty$ cases.

III. OUR MODEL

Then we consider the model of a non-Hermitian nodal-ring semimetal with the s -wave SC pairing term. With the Nambu basis $\psi = (c_{k,\uparrow}, c_{k,\downarrow}, c_{-k,\uparrow}^\dagger, c_{-k,\downarrow}^\dagger)^T$, the Bogoliubov-

de Gennes (BdG) Hamiltonian is

$$H(\mathbf{k}_\parallel, k_z) = (m_{xy} + 2B \cos k_z) \tau_z \sigma_x + i\gamma \tau_z \sigma_z + v_z \sin k_z \tau_0 \sigma_z - \Delta \tau_y \sigma_y, \quad (11)$$

where \mathbf{k}_\parallel is included in the m_{xy} term, Pauli matrices $\sigma_{x,y,z}$ and 2×2 identity matrix τ_0 act on the particle-hole degree of freedom. In the following part, we still set $2B = v_z$. (The general $2B \neq v_z$ cases are discussed in Sec. VIII.) Now we focus on the symmetries of the system. The Hamiltonian Eq. (11) satisfies time-reversal symmetry (TRS) $\mathcal{T}H^*(\mathbf{k}_\parallel, k_z)\mathcal{T}^{-1} = H(-\mathbf{k}_\parallel, -k_z)$, particle-hole symmetry (PHS) $\mathcal{C}H^T(\mathbf{k}_\parallel, k_z)\mathcal{C}^{-1} = -H(-\mathbf{k}_\parallel, -k_z)$, and chiral symmetry (CS) $\Gamma H^\dagger(\mathbf{k}_\parallel, k_z)\Gamma^{-1} = -H(\mathbf{k}_\parallel, k_z)$ with the following operators $\mathcal{T}/\mathcal{C}/\Gamma$:

$$\mathcal{T} = i\tau_z \sigma_x \mathcal{C} = \tau_x \Gamma = \mathcal{T}\mathcal{C} = -\tau_y \sigma_x. \quad (12)$$

Besides, the system also has the SLS $SH(\mathbf{k}_\parallel, k_z)\mathcal{S}^{-1} = -H(\mathbf{k}_\parallel, k_z)$ with $\mathcal{S} = \tau_z \sigma_y$. According to the non-Hermitian Altland-Zirnbauer classification [79], when the SC pairing term is finite, the system belongs to the BDI topological class and has SLS anti-commuting with TRS and PHS operators. Similar to Hermitian examples [80–82], when k_x and k_y are treated as sole parameters, this system is reduced to a quasi-1D model of this class and this quasi-1D model has a line gap. Then, the topological index of our quasi-1D model corresponds to a winding number from SLS. The Bloch winding number from SLS can be calculated from the following integral:

$$\nu = \frac{1}{4\pi i} \int_{-\pi}^{\pi} dk_z \text{Tr}[SH^{-1}(\mathbf{k}_\parallel, k_z) \partial_{k_z} H(\mathbf{k}_\parallel, k_z)]. \quad (13)$$

For $m_{xy} > 0$, the result is (see Appendix A)

$$\nu = \begin{cases} 0, & \text{if } 2B < M_- < M_+; \\ -1, & \text{if } M_- < 2B < M_+; \\ -2, & \text{if } M_- < M_+ < 2B, \end{cases} \quad (14)$$

where $M_\pm = |m_{xy} \pm \sqrt{\gamma^2 + \Delta^2}|$. When $m_{xy} < 0$, since $M_- > M_+$ in this case, we have $\nu = 0$ if $2B < M_+ < M_-$, $\nu = -1$ if $M_+ < 2B < M_-$, and $\nu = -2$ if $M_+ < M_- < 2B$. As we have explained in Sec. II, the topological phase transition in a system with the NHSE has to be investigated by the non-Bloch winding number rather than the Bloch one. However, we will show that the NHSE in our model is effectively removed by the finite SC pairing term, so the Bloch winding number in Eq. (13) can give the correct phase boundaries.

IV. INTRINSIC COUPLING BETWEEN THE DIFFERENT GBZS

In this section, we show that the coupling effect of the two different sub-GBZs induced by the SC term in our model, and this effect drives the sub-GBZs to BZ. To this end, we first rewrite the Eq. (11) as

$$H(k_z) = \begin{pmatrix} h_p & i\Delta\sigma_y \\ -i\Delta\sigma_y & h_H \end{pmatrix}, \quad (15)$$

with

$$h_p = (m_{xy} + 2B \cos k_z) \sigma_x + (i\gamma + v_z \sin k_z) \sigma_z,$$

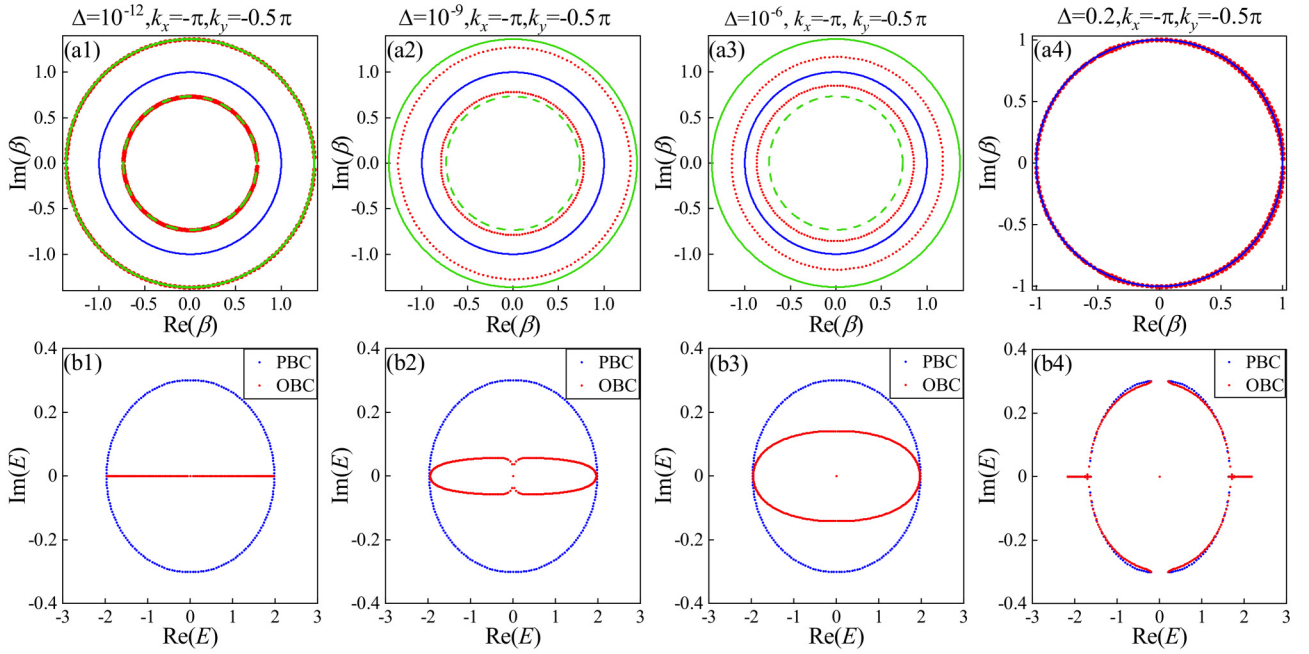


FIG. 2. (a1)–(a4) The sub-GBZs corresponding to the particle block h_p (green solid circle) and the hole block h_h (green dash circle). Red points denote total GBZs with different Δ s. The blue solid circle denotes BZ. (b1)–(b4) Complex eigenenergies under the PBC and OBC, which correspond to (a1)–(a4). Other parameters are $L = 80$, $\gamma = 0.3$, $v_z = 2B = 1$, $m = 0$.

$$h_H = -(m_{xy} + 2B \cos k_z) \sigma_x - (i\gamma - v_z \sin k_z) \sigma_z, \quad (16)$$

where P(H) denotes the particle (hole) parts in our model. We note that h_p is exactly the Hamiltonian of the non-Hermitian nodal-ring semimetal Eq. (1). So the sub-GBZ corresponding to h_p is given by Eq. (9), i.e.,

$$\beta_P(k_z) = \sqrt{\frac{m_{xy} - \gamma}{m_{xy} + \gamma}} e^{ik_z}. \quad (17)$$

For the hole part h_H , we can also obtain (see Appendix. B):

$$\beta_H(k_z) = \sqrt{\frac{m_{xy} + \gamma}{m_{xy} - \gamma}} e^{ik_z}. \quad (18)$$

Next, we investigate the coupling effect of the different sub-GBZs in our model. We start with $\Delta \rightarrow 0^+$ limit. The numerically solved total GBZs [83] (with the different $\Delta \rightarrow 0^+$) are shown in Figs. 2(a1)–2(a3). Unlike the examples in Refs. [77,78], the sub-GBZs corresponding to h_p and h_H are *intrinsically* coupled by the SC pairing term. And with the larger Δ , the total GBZ becomes closer to the BZ. The complex eigenenergies shown in Figs. 2(b1)–2(b3) also indicate similar results: Although the complex energies under the OBC are still different from those under the PBC, the bulk parts of the eigenenergies under the OBC become closer to those under PBC, which are quite different from the case of the system with the NHSE. These results show that the SC term induces coupling effects between the different sub-GBZs of corresponding to the h_p and h_H , and this coupling effect weakens the NHSE.

Then, for the finite Δ , Fig. 2(a4) shows that the GBZ and BZ are almost the same. And in Fig. 2(b4) we also find that the complex eigenenergies under PBC are almost the same as the bulk parts of those under OBC. Both results indicate that the

NHSE has been effectively destroyed by the coupling effect with the finite SC pairing term. In the next section, we will show that the convectional BBC is then reconstructed.

V. RECONSTRUCTED CONVENTIONAL BULK-BBC WITH THE FINITE Δ

To discuss the reconstructed BBC in our model, we still treat k_x and k_y as parameters, then the lattice Hamiltonian in the z direction is

$$\begin{aligned} H(\mathbf{k}_{\parallel}, k_z) = & \sum_{j,s} [(m_{xy} c_{j,s}^{\dagger} c_{j,-s} + B(c_{j,s}^{\dagger} c_{j+1,-s} + \text{H.c.})] \\ & + \sum_{j,s} \left[is\gamma c_{j,s}^{\dagger} c_{j,s} - \frac{1}{2} i v_z (s c_{j,s}^{\dagger} c_{j+1,s} - \text{H.c.}) \right] \\ & + \sum_{j,s} (s \Delta c_{j,s}^{\dagger} c_{j,-s} + \text{H.c.}), \end{aligned} \quad (19)$$

where the j is still the lattice index and the spin index is still denoted by $s = 1(-1)$.

We first identify the different phases by the Bloch winding number. For our model with $m = 3$, $2B = v_z = 1$, $\gamma = 0.3$, $k_x = -\pi$, and $\Delta = 0.2$. According to the result in Eq. (14), we have $v = 0$ when $k_- < |k_y| < k_+$, $v = -1$ when $k_+ < |k_y| < k_-$, and -2 for $|k_y| < k_+$, where $k_- = \arccos(-\sqrt{13}/10) \approx 0.62\pi$ and $k_+ = \arccos(\sqrt{13}/10) \approx 0.38\pi$. In Fig. 3(a), we find that the phase boundaries $k = |k_{\pm}|$ match well with the results of the OBC spectrum, which means that the conventional BBC is effectively reconstructed.

Then, to show our results more completely, we take different $k_x, k_y \in [-\pi, \pi]$ and apply the real-space winding number method (see Appendix C). The real-space winding number

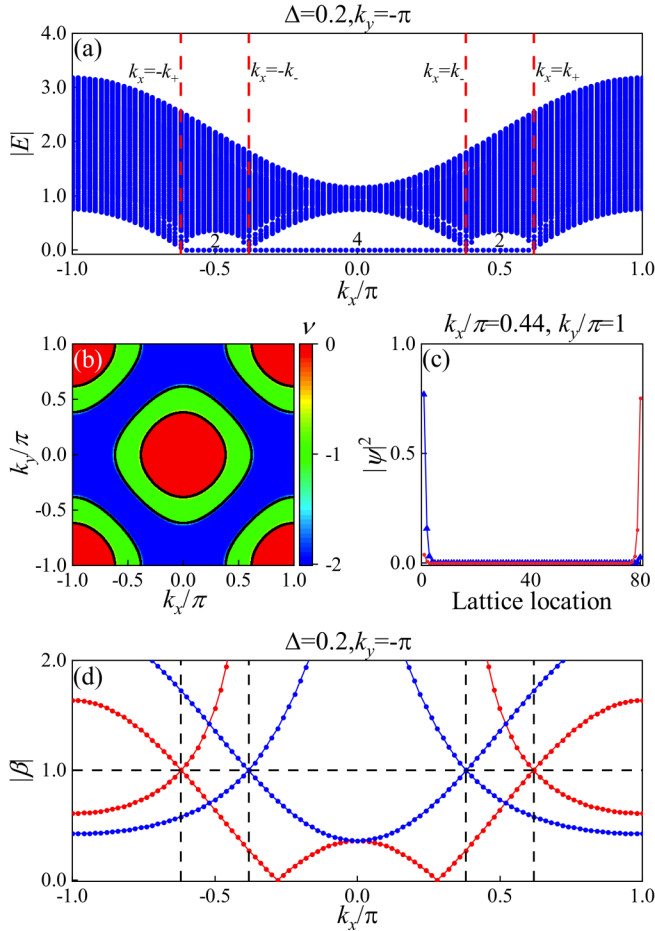


FIG. 3. (a) The OBC spectrum for our model with $\Delta = 0.2$. The red dashed lines are phase boundaries $k_x = \pm k_+$ and $k_x = \pm k_-$ given by the Bloch winding number. The numbers denote the number of the zero modes. (b) The real-space winding number as a function of k_x and k_y . The black solid lines are the phase boundaries given by the Bloch winding number. (c) Density distribution of zero modes for $k_x = 0.44\pi$ and $k_y = \pi$. (d) $\beta_{i,0} - k_x$ curves from Eq. (21), where each $\beta_{i,0}$ ($i = 1, 2, 3, 4$) is the solution of the characteristic equation Eq. (20) for $E = 0$. The two red (blue) lines denote $\beta_{1,0}$ and $\beta_{4,0}$ ($\beta_{2,0}$ and $\beta_{3,0}$). The four dashed perpendicular lines are $k_x = \pm k_+$ and $k_x = \pm k_-$. The horizontal line is $|\beta| = 1$. Other parameters are $L = 80$, $\gamma = 0.3$, $v_z = 2B = 1$, and $m = 0$.

under z direction as a function of k_x and k_y and the phase boundaries given by the Bloch winding number Eq. (14) are plotted in Fig. 3(b). We find that the Bloch winding number and the real-space winding number give the same phase boundaries, since the real-space winding number method is dual to the non-Bloch framework and gives the correct phase boundaries [75]. This result implies that the NHSE is removed in our model and the conventional BBC is reconstructed. In Fig. 3(c) we give the distribution of the edge modes along the z direction for $(k_x, k_y) = (0.44\pi, \pi)$. According to Fig. 3(c), this model is in a topological phase $\nu = -1$ and has two edge modes, which is consistent with the result in Fig. 3(b).

We also investigate the localization strength of the Majorana zero states. To this end, we still assume a trial function of the n_z th site along the z direction $\psi(k_{\parallel}, n_z) =$

$e^{i(k_x x + k_y y)}(\alpha_1, \alpha_2, \alpha_3, \alpha_4)^T \beta^{n_z}$ and substitute it to Eq. (19). For $E = 0$, the eigenequation $H\psi(k_{\parallel}, n_z) = 0$ leads to

$$\det[H(k_{\parallel}, \beta)] = \frac{[(m_{xy} + 2B\beta)^2 - \gamma^2 - \Delta^2]}{\beta^2} \times [(m_{xy}\beta + 2B)^2 - \beta^2(\gamma^2 + \Delta^2)] = 0. \quad (20)$$

This equation has four solutions:

$$\begin{aligned} \beta_{1,0} &= -\frac{m_{xy} + \sqrt{\Delta^2 + \gamma^2}}{2B}, & \beta_{3,0} &= -\frac{m_{xy} - \sqrt{\Delta^2 + \gamma^2}}{2B}, \\ \beta_{2,0} &= -\frac{2B}{m_{xy} - \sqrt{\gamma^2 + \Delta^2}}, & \beta_{4,0} &= -\frac{2B}{m_{xy} + \sqrt{\gamma^2 + \Delta^2}}, \end{aligned} \quad (21)$$

where the index 0 denotes that $\beta_{i,0}$ corresponds to the zero-edge modes rather than the GBZ. We note that all the solutions are real and $\beta_{1,0}\beta_{4,0} = 1$, $\beta_{2,0}\beta_{3,0} = 1$. In a system with the NHSE, the topological phase boundary should be given by each two $|\beta_{i,0}| = r_k$ [61], where r_k is the radius of the k -dependent solution about the GBZ [note that $\beta(k)$ can be written as $\beta(k) = r_k e^{ik}$ in Sec. II] in a complex plane. If $r_k \approx 1$, this condition is the same as that in the system without the NHSE. As we have shown in the previous parts of this section, the SC pairing term induces the coupling between two sub-GBZs of the particle and hole parts and this coupling makes the r_k close to 1, i.e., the total GBZ and BZ are the same. In Fig. 3(d), the $|\beta_{j,0}| - k_x$ curves show that at each phase boundary, the intersection of two $\beta_{j,0}$ occurs and the corresponding $|\beta_{j,0}| \approx 1$, which is similar to the case with the conventional BBC [84]. Thus this result also indicates that the convectional BBC is constructed.

VI. FINITE-SIZE EFFECT

For a system without the NHSE, the finite-size effect means that the coupling between zero modes on the two ends of the chain can open an energy gap due to the finite chain length [85]. Usually, this finite-size effect cannot change the whole complex eigenenergies of an open chain fundamentally. However, in a system with the CNHSE, since the eigenenergies under the OBC changes dramatically and the size-dependent zero modes may occur with the increasing size of the system [77], the meaning of the finite-size effect changes a lot. To show these differences, we numerically calculate the eigenenergies of the lattice Hamiltonian Eq. (19) with the different strength of the SC pairing term and open chain length L . The results are also plotted in Fig. 4.

We first consider the $\Delta = 0.01$ case. From Figs. 4(a1)–4(a3) we find that for the $\Delta \rightarrow 0^+$ case, as the system size L increases, the eigenenergies under OBC change a lot while the ones under PBC are not sensitive to size. Besides, the *size-dependent* zero modes occur. These results indicate that for the $\Delta \rightarrow 0^+$ case, the CNHSE exists in our model.

Then, for $\Delta = 0.2$, Figs. 4(b1)–4(b3) show that the eigenenergies under the OBC only change a little with different size L , and zero-modes are *size-independent*, which means that the finite-size effect does not change the eigenenergies under the OBC dramatically and that the NHSE is much

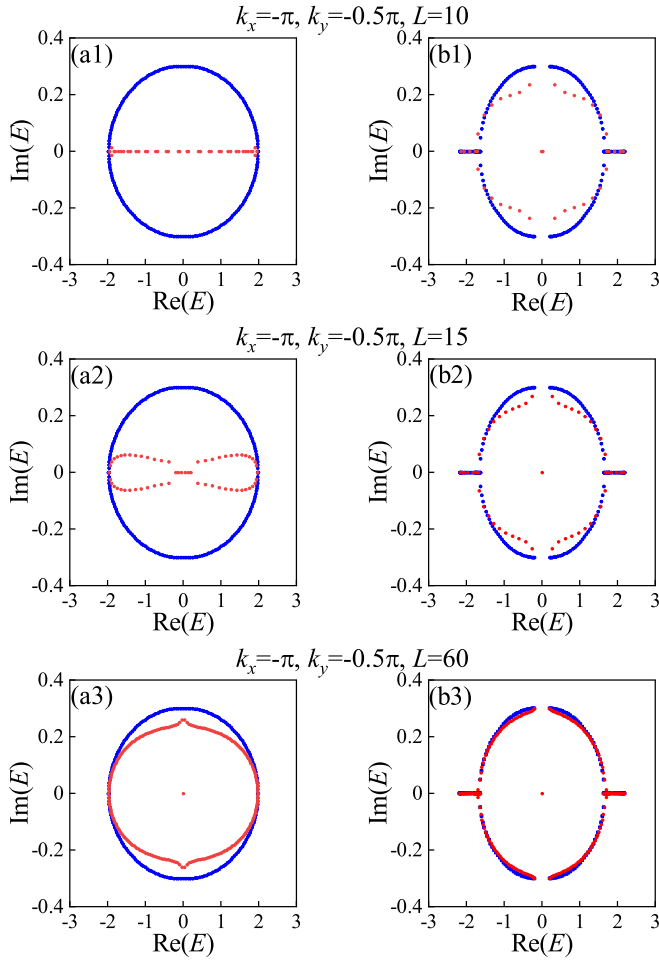


FIG. 4. (a1)–(a3) Complex eigenenergies for $\Delta = 0.01$. (b1)–(b3) Complex eigenenergies for $\Delta = 0.2$. The blue (red) points denote eigenenergies under PBC (OBC). The system length $L = 10, 15$, and 60 . Other parameters are $L = 80$, $\gamma = 0.3$, $v_z = 2B = 1$, and $m = 0$.

weaker when the Δ is finite. This result is consistent with that obtained from the GBZ analysis in Sec. IV.

VII. POSSIBLE EXPERIMENTAL REGIME

In this section, we consider a possible experimental set up in the RLC circuit as illustrated in Fig. 5. Since the purpose is to *simulating our model*, we can independently consider x , y , and z directions and stimulate the corresponding Hamiltonian $H_{x,y,z}$, as in Fig. 5(a) and 5(b). Then the total Hamiltonian $H = H_x + H_y + H_z$ can be simulated.

Now we discuss details. In the circuit shown in Figs. 5(a) and 5(b), our model is divided into two parts simulating the particle and hole bands correspondingly, and each “lattice” is combined with four nodes (1,2,3,4), which corresponds to the Nambu basis $(c_{i,\uparrow}, c_{i,\downarrow}, c_{i,\uparrow}^\dagger, c_{i,\downarrow}^\dagger)$ for the i th lattice. The “spin-flipping hopping term” can be realized by the capacitors C_0, C_1 and inductors L_0, L_1 [86,87], and the capacitors C_Δ and the inductors L_Δ connecting two parts play a role as the “pairing term” [88]. As for the loss-and-gain term, we can simulate them by the grounded resistor [89]. The operational

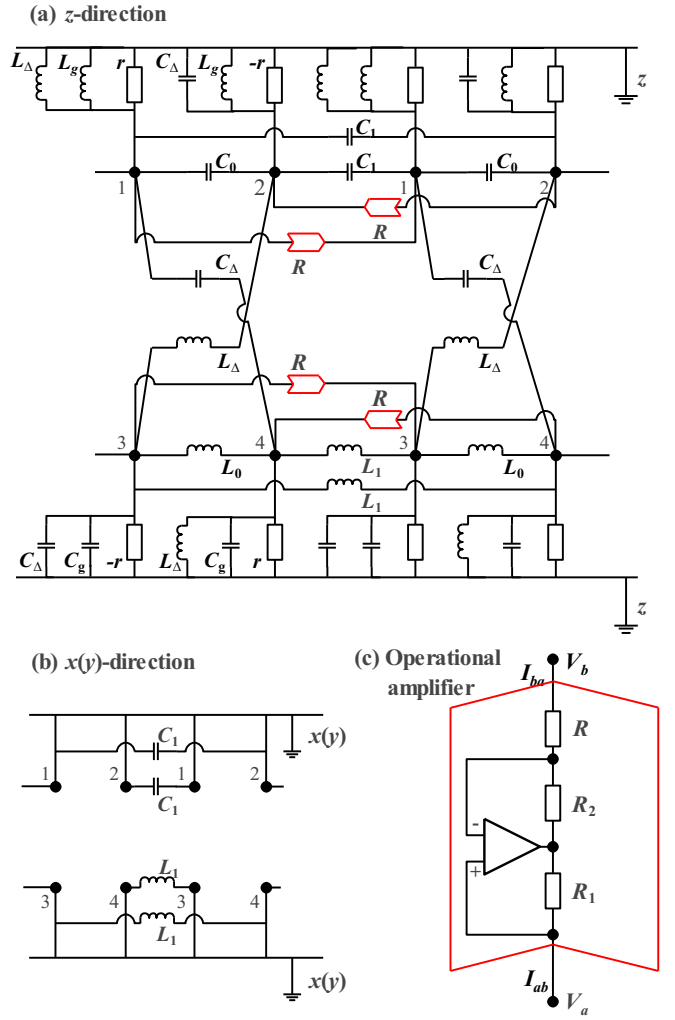


FIG. 5. Electric circuit simulating the non-Hermitian nodal-ring semimetal with the s -wave pairing. The circuit consists of two parts. In this electron circuit, each unit cell has four nodes and these nodes are labeled by 1–4. The part containing 1 and 2 (3 and 4) nodes simulates the particle (hole) band. (a) The circuit realization of the terms in the z direction. The operational amplifier is colored red. (b) The circuit realization of the terms in the $x(y)$ direction. (c) Circuit structure of an operational amplifier shown in (a), where $R_1 = R_2$ and the resistive parameter is R .

amplifier, which acts as the negative impedance converters with current inversion (INIC), is also applied to this setup. In the operational amplifier shown in Fig. 5(c), the resistance is R for the forward current and $-R$ for the backward current as long as $R_1 = R_2$ [88,90]. Due to these properties, the operational amplifier can introduce the resistor $-r$ required in the loss-and-gain term and the spin-conserved term like $\sum_s \frac{i v_z s}{2} (c_{i,s}^\dagger c_{i+1,s} - c_{i+1,s}^\dagger c_{i,s})$ (where $s = \pm 1$ denotes the spin degree of freedom).

Then, according to Kirchhoff current law, when we apply a time-dependent voltage $V(t) = V(0)e^{i\omega t}$ to a circuit, we have [86,87]

$$I_a = \sum_b \left[i\omega C_{ab} + \frac{1}{R_{ab}} + \frac{1}{i\omega L_{ab}} \right] V_b = J_{ab}(\omega) V_b, \quad (22)$$

where I_a is the current flowing out of a node a , V_b denotes the voltage across nodes a and b , and C_{ab} , R_{ab} , and L_{ab} are the corresponding capacitance, resistance, and inverse conductance, respectively. We can also rewrite Eq. (22) in the matrix form:

$$\mathbf{I} = \left[i\omega\mathbf{C} + \mathbf{R}^{-1} + \frac{\mathbf{L}'}{i\omega} \right] \mathbf{V} = \mathbf{J}(\omega)\mathbf{V}, \quad (23)$$

where $\mathbf{J}(\omega)$ is the circuit Laplacian, and the element of the matrix \mathbf{L}' corresponding the conductor between nodes a and b is L_{ab}^{-1} .

For the RLC circuit shown in Fig. 5, the corresponding Laplacian is

$$J_{ab}(\omega) = i\omega \begin{pmatrix} j_1(\omega) & f(\omega) \\ f^T(\omega) & j_2(\omega) \end{pmatrix}, \quad (24)$$

with

$$j_1(\omega) = \left(C_0 + 6C_1 - \frac{1}{\omega^2 L_g} + C_\Delta - \frac{1}{\omega^2 L_\Delta} \right) I - \left(C_0 + 2C_1 \sum_{\alpha=x,y,z} \cos k_\alpha \right) \sigma_x - \left(\frac{\sin k_x}{R} - \frac{i}{r} \right) \sigma_z, \quad (25)$$

$$j_2(\omega) = \left(C_g - \frac{1}{\omega^2 L_0} - \frac{6}{\omega^2 L_1} + C_\Delta - \frac{1}{\omega^2 L_\Delta} \right) I + \left(\frac{1}{\omega_0} + \frac{2}{\omega_1} \sum_{\alpha=x,y,z} \cos k_\alpha \right) \sigma_x - \left(\frac{\sin k_x}{R} + \frac{i}{r} \right) \sigma_z, \quad (26)$$

$$f(\omega) = \begin{pmatrix} 0 & -C_\Delta \\ \frac{1}{\omega^2 L_\Delta} & 0 \end{pmatrix}. \quad (27)$$

By comparing the circuit Laplacian to the Bloch Hamiltonian Eq. (1), we have

$$\begin{aligned} \omega^2 &= \frac{1}{C_0 L_0} = \frac{1}{C_1 L_1} = \frac{1}{C_\Delta L_\Delta} \\ &= \frac{1}{(C_0 + 6C_1)L_g} = \frac{1}{C_g} \left(\frac{1}{L_0} + \frac{6}{L_1} \right). \end{aligned} \quad (28)$$

Here the terms $6C_1$ and $6/L_1$ are induced by the spin-flipping hopping term $\cos k_\alpha \sigma_x$ in $\alpha = x, y$, and z directions. With Eq. (28), the model parameters in Eq. (27) and Eq. (11) has the following correspondence:

$$\begin{aligned} C_\Delta &= -\Delta, C_0 = -m_0, C_1 = -B, \\ v_z &= \frac{1}{R}, \gamma = \frac{1}{r}. \end{aligned} \quad (29)$$

Now it is possible to simulate a non-Hermitian nodal-ring semimetal with the s -wave pairing.

VIII. DISCUSSION AND CONCLUSION

We first discuss whether the reconstructed BBC is valid for the $2B \neq v_z$ cases. In this work, our main point is that the coupling effect induced by the SC term makes the GBZ very close to the BZ and the different NHSE localizations can be perfectly canceled. Then the conventional BBC effectively works again. For many $2B \neq v_z$ cases, the condition that the SC term makes the GBZ very close to the BZ is usually

not satisfied well, which means that the different NHSE localizations of the subbands cannot be perfectly canceled. So generally speaking, the conventional BBC cannot be rebuilt in these cases, i.e., the phase boundaries given by the Bloch winding number are different from the real phase boundaries. This point also means the reconstructed conventional BBC is more fragile than the original conventional BBC.

In summary, based on the knowledge of GBZ framework, we investigate the BBC of a non-Hermitian nodal-ring semimetal with s -wave SC pairing term. As long as the s -wave pairing term is nonzero, the GBZs of particle and hole parts will be coupled and this coupling drives them to the BZ. When the SC term is finite, we show that the coupling effect makes it possible to perfectly remove the NHSE in our model and the total GBZ of our model becomes the same as the BZ. In this case, the quasi-1D Bloch winding number predicts the number of Majorana zero modes and the phase boundaries faithfully, which means the convectional BBC is reconstructed in our model. Our results may be generalized to the topological systems with the coupled high-order NHSE [64,91]. It is also interesting to investigate the effects of the interaction and disorders in this reconstructed BBC.

ACKNOWLEDGMENTS

We are grateful to Huaiqiang Wang and Hao Geng for helpful discussions. This work was supported by the State Key Program for Basic Researches of China under Grant No. 2017YFA0303203 (D.Y.X.) and the National Natural Science Foundation of China under Grant No. 11974168 (L.S.).

APPENDIX A: CALCULATION DETAILS OF THE BLOCH WINDING NUMBER

We calculate the Bloch winding number from SLS with SLS symmetry operator $\mathcal{S} = \tau_z \sigma_y$, which is given by Eq. (13) in the main text. After the following unitary transformation,

$$U = \frac{1}{2} [\tau_0 \otimes (\sigma_y + \sigma_0) + \tau_x \otimes (\sigma_y - \sigma_0)], \quad (A1)$$

then it follows that

$$USU^\dagger = \tau_z \otimes \sigma_0 \quad H'(k) = UH(k)U^\dagger = \begin{pmatrix} 0 & h_+(k) \\ h_-(k) & 0 \end{pmatrix}, \quad (A2)$$

with

$$h_\pm(k) = \begin{pmatrix} -v_z \sin k_z \pm i(\Delta + m) & \pm\gamma \\ \pm\gamma & v_z \sin k_z \pm i(\Delta - m) \end{pmatrix}, \quad (A3)$$

where $m = m_0 + 2B(\cos k_x + \cos k_y + \cos k_z)$. Next, we have

$$\begin{aligned} \nu &= \frac{1}{4\pi i} \oint_{\text{BZ}} dk \text{Tr}[\tau_z H'^{-1}(k) \partial_k H'(k)] \\ &= \frac{1}{4\pi i} \int_{-\pi}^{\pi} d \ln[Z^*(k_z)] - d \ln[Z(k_z)] \\ &= \frac{1}{2} (W_+ - W_-), \end{aligned} \quad (A4)$$

where $Z(k_z) = (v_z \sin k_z - im)^2 + \gamma^2 + \Delta^2$. For the $2B = v_z$ case, the W_- is given by the following integral:

$$\begin{aligned} W_- &= \frac{1}{4\pi i} \oint_{BZ} dk \frac{-4B(m_{xy} + 2Be^{ik_z})e^{ik_z}}{(\gamma^2 + \Delta^2) - (m_{xy} + 2Be^{ik_z})^2} \\ &= \frac{1}{4\pi i} \oint_{BZ} \frac{2(z + \frac{m_{xy}}{2B})}{(z + z_+)(z + z_-)} \end{aligned} \quad (A5)$$

with $z_{\pm} = (m_{xy} \pm \sqrt{\gamma^2 + \Delta^2})/(2B)$. Obviously this contour integral is dependent on the number of the poles. By comparing the $|m_{xy} \pm \sqrt{\gamma^2 + \Delta^2}|$ and $2B$, we can obtain the Eq. (14) in the main text.

APPENDIX B: SUB-GBZ SOLUTION FOR THE HOLE BLOCK

According to Refs. [67,69], to obtain the sub-GBZ of the hole block h_H , we have to deal with the characteristic equation of each block:

$$\det[EI - h_H(\beta_H)] = 0. \quad (B1)$$

For the hole Block in Eq. (16) of the main text, with the replacement $e^{ik} \rightarrow \beta$, this characteristic equation leads to

$$E_H^2 = \left[m_{xy} + B \left(\beta_H + \frac{1}{\beta_H} \right) \right]^2 + \left[\frac{v_z}{2i} \left(\beta_H - \frac{1}{\beta_H} \right) - i\gamma \right]^2. \quad (B2)$$

If $B = v_z/2 = t$, we have

$$2t(m_{xy} - \gamma)\beta^2 + (m_{xy}^2 - \gamma^2 + 4t^2 - E^2)\beta + 2t(m_{xy} + \gamma) = 0, \quad (B3)$$

so the two solutions of the equation β_1 and β_2 satisfy

$$\beta_1 \beta_2 = \frac{m_{xy} + \gamma}{m_{xy} - \gamma}. \quad (B4)$$

According to the results in Refs. [67,69], the sub-GBZ solution in this model requires $|\beta_1| = |\beta_2|$. Combining with

Eq. (B4), we obtain that

$$|\beta_H| = |\beta_{1,H}| = |\beta_{2,H}| = \sqrt{\left| \frac{m_{xy} + \gamma}{m_{xy} - \gamma} \right|}. \quad (B5)$$

Since a GBZ solutions can always be written as $\beta(k) = |\beta(k)|e^{ik}$, we have Eq. (18) in the main text.

APPENDIX C: REAL-SPACE WINDING NUMBER FROM SLS

In this part, we briefly review the real-space winding number method, as the example in Ref. [75], if a real-space Hamiltonian H with N unit cells satisfies SLS. After diagonalizing H , one can obtain two SLS parts: $H|nR, \pm\rangle = \pm E_R|nR, \pm\rangle$ with $|nR, +\rangle = \mathcal{S}|nR, -\rangle$, where $\mathcal{S} = \tau_z \otimes \mathbb{1}_N \otimes \sigma_y$ is the SLS operator and n is the band index. The corresponding left eigenvectors $\langle nL, s, \pm|$ can be obtained from the columns of $(T^{-1})^\dagger$ by writing $H = T\Gamma T^{-1}$ with the diagonal matrix Γ . Under the OBC we can introduce open-boundary matrix Q ,

$$Q = \sum_n (|nR, +\rangle\langle nL, +| - |nR, -\rangle\langle nL, -|). \quad (C1)$$

Here \sum_n is the sum over the eigenstates. Then the real-space winding number is defined as:

$$\nu_s = \frac{1}{4L'} \text{Tr}'(SQ[Q, X]) + \text{H.c.}, \quad (C2)$$

where X is the coordinate operator, and the chain length $L = L' + 2l$ includes the middle interval with length L' and two boundary intervals $1 \leq x \leq l$ and $l + L' + 1 \leq x \leq l$. In the $L \rightarrow \infty$ limit, the ν approaches to 1 when a system is topological and 0 for the trivial phase. And the Tr' stands for the trace over middle interval including sublattice and Nambu index.

-
- [1] M. Z. Hasan and C. L. Kane, *Rev. Mod. Phys.* **82**, 3045 (2010).
 - [2] X.-L. Qi and S. C. Zhang, *Rev. Mod. Phys.* **83**, 1057 (2011).
 - [3] C. K. Chiu, J. C. Y. Teo, A. P. Schnyder, and S. Ryu, *Rev. Mod. Phys.* **88**, 035005 (2016).
 - [4] C. L. Kane and E. J. Mele, *Phys. Rev. Lett.* **95**, 226801 (2005).
 - [5] C. L. Kane and E. J. Mele, *Phys. Rev. Lett.* **95**, 146802 (2005).
 - [6] B. A. Bernevig, T. L. Hughes, and S.-C. Zhang, *Science* **314**, 1757 (2006).
 - [7] M. König, S. Wiedmann, C. Brune, A. Roth, H. Buhmann, L. W. Molenkamp, X.-L. Qi, and S.-C. Zhang, *Science* **318**, 766 (2007).
 - [8] L. Fu, C. L. Kane, and E. J. Mele, *Phys. Rev. Lett.* **98**, 106803 (2007).
 - [9] L. Fu and C. L. Kane, *Phys. Rev. B* **76**, 045302 (2007).
 - [10] Y. L. Chen, J. G. Analytis, J.-H. Chu, Z. K. Liu, S.-K. Mo, X. L. Qi, H. J. Zhang, D. H. Lu, X. Dai, Z. Fang, S. C. Zhang, I. R. Fisher, Z. Hussain, and Z.-X. Shen, *Science* **325**, 178 (2009).
 - [11] H. J. Zhang, C. X. Liu, X. L. Qi, X. Dai, Z. Fang, and S. C. Zhang, *Nat. Phys.* **5**, 438 (2009).
 - [12] A. Y. Kitaev, *Phys. Usp.* **44**, 131 (2001).
 - [13] J. Alicea, *Rep. Prog. Phys.* **75**, 076501 (2012).
 - [14] C. W. J. Beenakker, *Rev. Mod. Phys.* **87**, 1037 (2015).
 - [15] M. Sato and S. Fujimoto, *J. Phys. Soc. Jpn.* **85**, 072001 (2016).
 - [16] L. Fu and C. L. Kane, *Phys. Rev. Lett.* **100**, 096407 (2008).
 - [17] X.-L. Qi, T. L. Hughes, and S.-C. Zhang, *Phys. Rev. B* **82**, 184516 (2010).
 - [18] J. Wang, Q. Zhou, B. Lian, and S.-C. Zhang, *Phys. Rev. B* **92**, 064520 (2015).
 - [19] R. M. Lutchyn, J. D. Sau, and S. Das Sarma, *Phys. Rev. Lett.* **105**, 077001 (2010).
 - [20] Y. Oreg, G. Refael, and F. von Oppen, *Phys. Rev. Lett.* **105**, 177002 (2010).
 - [21] V. Mourik, K. Zuo, S. M. Frolov, S. R. Plissard, E. P. A. M. Bakkers, and L. P. Kouwenhoven, *Science* **336**, 1003 (2012).

- [22] P. Zhang, K. Yaji, T. Hashimoto, Y. Ota, T. Kondo, K. Okazaki, Z. Wang, J. Wen, G. D. Gu, H. Ding, and S. Shin, *Science* **360**, 182 (2018).
- [23] D. F. Wang, L. Y. Kong, P. Fan, H. Chen, S. Y. Zhu, W. Y. Liu, L. Cao, Y. J. Sun, S. X. Du, J. Schneeloch, R. D. Zhong, G. D. Gu, L. Fu, H. Ding, and H.-J. Gao, *Science* **362**, 333 (2018).
- [24] H.-H. Sun, K.-W. Zhang, L.-H. Hu, C. Li, G.-Y. Wang, H.-Y. Ma, Z.-A. Xu, C.-L. Gao, D.-D. Guan, Y.-Y. Li, C. Liu, D. Qian, Y. Zhou, L. Fu, S.-C. Li, F.-C. Zhang, and J.-F. Jia, *Phys. Rev. Lett.* **116**, 257003 (2016).
- [25] N. P. Armitage, E. J. Mele, and A. Vishwanath, *Rev. Mod. Phys.* **90**, 015001 (2018).
- [26] A. A. Burkov and L. Balents, *Phys. Rev. Lett.* **107**, 127205 (2011).
- [27] A. A. Burkov, M. D. Hook, and L. Balents, *Phys. Rev. B* **84**, 235126 (2011).
- [28] X. Wan, A. M. Turner, A. Vishwanath, and S. Y. Savrasov, *Phys. Rev. B* **83**, 205101 (2011).
- [29] S.-Y. Xu, I. Belopolski, N. Alidoust, M. Neupane, G. Bian, C. Zhang, R. Sankar, G. Chang, Z. Yuan, C.-C. Lee *et al.*, *Science* **349**, 613 (2015).
- [30] B. Q. Lv, H. M. Weng, B. B. Fu, X. P. Wang, H. Miao, J. Ma, P. Richard, X. C. Huang, L. X. Zhao, G. F. Chen, Z. Fang, X. Dai, T. Qian, and H. Ding, *Phys. Rev. X* **5**, 031013 (2015).
- [31] C. Fang, Y. Chen, H.-Y. Kee, and L. Fu, *Phys. Rev. B* **92**, 081201(R) (2015).
- [32] Y. Kim, B. J. Wieder, C. L. Kane, and A. M. Rappe, *Phys. Rev. Lett.* **115**, 036806 (2015).
- [33] R. Yu, H. Weng, Z. Fang, X. Dai, and X. Hu, *Phys. Rev. Lett.* **115**, 036807 (2015).
- [34] Z. Yan, R. Bi, H. Shen, L. Lu, S.-C. Zhang, and Z. Wang, *Phys. Rev. B* **96**, 041103(R) (2017).
- [35] W. Chen, H.-Z. Lu, and J.-M. Hou, *Phys. Rev. B* **96**, 041102(R) (2017).
- [36] G. Bian, T.-R. Chang, R. Sankar, S.-Y. Xu, H. Zheng, T. Neupert, C.-K. Chiu, S.-M. Huang, G. Chang, I. Belopolski *et al.*, *Nat. Commun.* **7**, 10556 (2016).
- [37] L. M. Schoop, M. N. Ali, C. Straßer, A. Topp, A. Varykhalov, D. Marchenko, V. Duppel, S. S. P. Parkin, B. V. Lotsch, and C. R. Ast, *Nat. Commun.* **7**, 11696 (2016).
- [38] X. Wang, X. Pan, M. Gao, J. Yu, J. Jiang, J. Zhang, H. Zuo, M. Zhang, Z. Wei *et al.*, *Adv. Electron. Mater.* **2**, 1600228 (2016).
- [39] Z. K. Liu, B. Zhou, Y. Zhang, Z. J. Wang, H. M. Weng, D. Prabhakaran, S.-K. Mo, Z. X. Shen, Z. Fang, X. Dai, Z. Hussain, and Y. L. Chen, *Science* **343**, 864 (2014).
- [40] I. Rotter, *J. Phys. A* **42**, 153001 (2009).
- [41] H. J. Carmichael, *Phys. Rev. Lett.* **70**, 2273 (1993).
- [42] B. Zhen, C. W. Hsu, Y. Igarashi, L. Lu, I. Kaminer, A. Pick, S.-L. Chua, J. D. Joannopoulos, and M. Soljacic, *Nature (London)* **525**, 354 (2015).
- [43] S. Malzard, C. Poli, and H. Schomerus, *Phys. Rev. Lett.* **115**, 200402 (2015).
- [44] T. E. Lee and C.-K. Chan, *Phys. Rev. X* **4**, 041001 (2014).
- [45] S. Diehl, E. Rico, M. A. Baranov, and P. Zoller, *Nat. Phys.* **7**, 971 (2011).
- [46] Y. Choi, S. Kang, S. Lim, W. Kim, J.-R. Kim, J.-H. Lee, and K. An, *Phys. Rev. Lett.* **104**, 153601 (2010).
- [47] J. Li, A. K. Harter, J. Liu, L. de Melo, Y. N. Joglekar, and L. Luo, *Nat. Commun.* **10**, 855 (2019).
- [48] Y. Xu, S.-T. Wang, and L.-M. Duan, *Phys. Rev. Lett.* **118**, 045701 (2017).
- [49] L. Li, C. H. Lee, and J. Gong, *Phys. Rev. Lett.* **124**, 250402 (2020).
- [50] L. Pan, X. Chen, Y. Chen, and H. Zhai, *Nat. Phys.* **16**, 767 (2020).
- [51] M. Nakagawa, N. Kawakami, and M. Ueda, *Phys. Rev. Lett.* **121**, 203001 (2018).
- [52] K. Yamamoto, M. Nakagawa, K. Adachi, K. Takasan, M. Ueda, and N. Kawakami, *Phys. Rev. Lett.* **123**, 123601 (2019).
- [53] P. He, J.-H. Fu, D.-W. Zhang, and S.-L. Zhu, *Phys. Rev. A* **102**, 023308 (2020).
- [54] V. Kozii and L. Fu, *arXiv:1708.05841*.
- [55] M. Papaj, H. Isobe, and L. Fu, *Phys. Rev. B* **99**, 201107(R) (2019).
- [56] A. A. Zyuzin and A. Y. Zyuzin, *Phys. Rev. B* **97**, 041203(R) (2018).
- [57] E. J. Bergholtz and J. C. Budich, *Phys. Rev. Research* **1**, 012003(R) (2019).
- [58] H. Shen and L. Fu, *Phys. Rev. Lett.* **121**, 026403 (2018).
- [59] T. M. Philip, M. R. Hirsbrunner, and M. J. Gilbert, *Phys. Rev. B* **98**, 155430 (2018).
- [60] S. Yao, F. Song, and Z. Wang, *Phys. Rev. Lett.* **121**, 136802 (2018).
- [61] S. Yao and Z. Wang, *Phys. Rev. Lett.* **121**, 086803 (2018).
- [62] F. K. Kunst, E. Edvardsson, J. C. Budich, and E. J. Bergholtz, *Phys. Rev. Lett.* **121**, 026808 (2018).
- [63] Z. Gong, Y. Ashida, K. Kawabata, K. Takasan, S. Higashikawa, and M. Ueda, *Phys. Rev. X* **8**, 031079 (2018).
- [64] R. Okugawa, R. Takahashi, and K. Yokomizo, *Phys. Rev. B* **102**, 241202(R) (2020).
- [65] F. Song, S. Yao, and Z. Wang, *Phys. Rev. Lett.* **123**, 170401 (2019).
- [66] Y. Yi and Z. Yang, *Phys. Rev. Lett.* **125**, 186802 (2020).
- [67] K. Yokomizo and S. Murakami, *Phys. Rev. Lett.* **123**, 066404 (2019).
- [68] K. Zhang, Z. Yang, and C. Fang, *Phys. Rev. Lett.* **125**, 126402 (2020).
- [69] Z. Yang, K. Zhang, C. Fang, and J. Hu, *Phys. Rev. Lett.* **125**, 226402 (2020).
- [70] Y. Xiong, *J. Phys. Commun.* **2**, 035043 (2018).
- [71] H. Wang, J. Ruan, and H. Zhang, *Phys. Rev. B* **99**, 075130 (2019).
- [72] Z. Zhang, Z. Yang, and J. Hu, *Phys. Rev. B* **102**, 045412 (2020).
- [73] X. Zhu, H. Wang, S. K. Gupta, H. Zhang, B. Xie, M. Lu, and Y. Chen, *Phys. Rev. Research* **2**, 013280 (2020).
- [74] L. Xiao, T. Deng, K. Wang, G. Zhu, Z. Wang, W. Yi, and P. Xue, *Nat. Phys.* **16**, 761 (2020).
- [75] F. Song, S. Yao, and Z. Wang, *Phys. Rev. Lett.* **123**, 246801 (2019).
- [76] S. Longhi, *Phys. Rev. Research* **1**, 023013 (2019).
- [77] L. Li, C. H. Lee, S. Mu, and J. Gong, *Nat. Commun.* **11**, 5491 (2020).
- [78] N. Okuma and M. Sato, *Phys. Rev. Lett.* **123**, 097701 (2019).
- [79] K. Kawabata, K. Shiozaki, M. Ueda, and M. Sato, *Phys. Rev. X* **9**, 041015 (2019).

- [80] P.-H. Fu, J.-F. Liu, and J. Wu, [Phys. Rev. B **102**, 075430 \(2020\)](#).
- [81] R. W. Bomantara, G. N. Raghava, L. Zhou, and J. Gong, [Phys. Rev. E **93**, 022209 \(2016\)](#).
- [82] H.-Q. Wang, M. N. Chen, R. W. Bomantara, J. Gong, and D. Y. Xing, [Phys. Rev. B **95**, 075136 \(2017\)](#).
- [83] Since the GBZ is related with the bulk states, in Fig. 2 the corresponding β solution of the zero edge modes in process of numerically solving GBZ has been ignored.
- [84] H. Menke and M. M. Hirschmann, [Phys. Rev. B **95**, 174506 \(2017\)](#).
- [85] C.-B. Hua, R. Chen, D.-H. Xu, and B. Zhou, [Phys. Rev. B **100**, 205302 \(2019\)](#).
- [86] S. Imhof, C. Berger, F. Bayer, J. Brehm, L. Molenkamp, T. Kiessling, F. Schindler, C. H. Lee, M. Greiter, T. Neupert, and R. Thomale, [Nat. Phys. **14**, 925 \(2018\)](#).
- [87] C. H. Lee, S. Imhof, C. Berger, F. Bayer, J. Brehm, L. W. Molenkamp, T. Kiessling, and R. Thomale, [Commun. Phys. **1**, 39 \(2018\)](#).
- [88] M. Ezawa, [Phys. Rev. B **100**, 045407 \(2019\)](#).
- [89] S. Liu, S. Ma, C. Yang, L. Zhang, W. Gao, Y. J. Xiang, T. J. Cui, and S. Zhang, [Phys. Rev. Appl. **13**, 014047 \(2020\)](#).
- [90] T. Hofmann, T. Helbig, C. H. Lee, M. Greiter, and R. Thomale, [Phys. Rev. Lett. **122**, 247702 \(2019\)](#).
- [91] K. Kawabata, M. Sato, and K. Shiozaki, [Phys. Rev. B **102**, 205118 \(2020\)](#).